JOURNAL OF GEOPHYSICAL RESEARCH, VOL. 106, NO. D18, PAGES 20735–20747, SEPTEMBER 27, 2001

Four years of continuous surface aerosol measurements from the Department of Energy's Atmospheric Radiation Measurement Program Southern Great Plains Cloud and Radiation Testbed site

P. J. Sheridan, D. J. Delene, and J. A. Ogren
Climate Monitoring and Diagnostics Laboratory, NOAA, Boulder, Colorado, USA

Abstract. Continuous measurements of the optical and microphysical properties of aerosol particles have been made at the Department of Energy's Atmospheric Radiation Measurement Program Southern Great Plains Cloud and Radiation Testbed (CART) site covering the 4-year period from July 1996 through June 2000. Hourly, daily, and monthly statistics have been calculated that illustrate aerosol variability over a range of timescales. A pronounced peak in total particle number, centered on the midafternoon hours (local time), is evident in the hourly statistics. A broad early morning peak in the concentration of particles >0.1-μm aerodynamic diameter corresponds with a similar peak in aerosol light-scattering coefficient, σ_{sp}. No strong cycles were observed in the daily statistics, suggesting that day of the week has only a minor influence on the observed aerosol variability. The σ_{sp} at a wavelength of 550 nm for the 4-year period showed a median value of 33 Mm^{-1} and was highest in February and August. The median fraction of aerosol light scattering at 550 nm due to particles <1-μm aerodynamic diameter was 0.85 over the entire record. The median aerosol light absorption coefficient, σ_{ap}, for the 4-year period was ~1.5 Mm^{-1} and was observed to be highest in late summer and autumn. The σ_{ap} showed an increasing trend of nearly 0.5 Mm^{-1} yr, possibly due to increased agricultural field burning in the area. The occurrence of an autumn decrease in single-scattering albedo, ω_0, was observed and may be caused by regional-scale agricultural or transportation activities or seasonal changes in atmospheric flow patterns. The median value for ω_0 over the 4-year period was 0.95, but this value has decreased ~1–2% yr^{-1} presumably due to increased agricultural burning. Numerous field fires during the second half of 1999 influenced the surface aerosol at the CART site causing substantial variability of aerosol optical properties. The aerosol hygroscopic growth factor (f(RH)), corresponding to a relative humidity increase of 40–85%, showed a median value of 1.83 for 1999, although much lower values were observed during periods that were probably influenced by locally generated smoke and dust aerosols (median f(RH) = 1.55 and 1.59, respectively).

1. Introduction

The perturbation of climate through the scattering and absorption of solar radiation by anthropogenic aerosols has been termed direct aerosol radiative forcing. This forcing has been estimated globally to be of similar magnitude and opposite sign (i.e., a negative forcing) to greenhouse gas forcing [*Charlson et al.*, 1992; *Kiehl and Briegleb*, 1993]. A more recent assessment has reached similar conclusions, although the magnitude of the global estimate of direct aerosol radiative forcing was lowered from the previous estimates [*Intergovernmental Panel on Climate Change (IPCC)*, 1996]. While the global estimates are useful for planetary radiation balance calculations, direct aerosol radiative forcing acts primarily on local to regional scales due to the nonuniform distribution of aerosol particles in the atmosphere. Thus it is unrealistic to believe that aerosol climate forcing effects will offset anthropogenic greenhouse warming in all locations. The combined effect will likely be a net atmospheric heating in some areas while others may experience a net cooling, and the long-term climatic impacts of these changes are not well understood [*Penner et al.*, 1994].

In order to make local estimates of direct aerosol radiative forcing, several key aerosol optical properties (AOPs) must be measured or estimated. These include the relative amounts of light scattering and absorption by the aerosol, the fraction of the incident solar radiation that is scattered upward to space by the suspended particles (the upscatter fraction β), and the optical thickness of the aerosol. Knowledge of these AOPs along with estimates of solar, atmospheric, and surface properties permits calculation of direct aerosol radiative forcing effects [*Haywood and Shine*, 1995]. To date, with the exception of aerosol optical thickness, there are relatively few measurements of these important aerosol properties. A few surface aerosol-monitoring sites that measure these aerosol properties have been in operation for a few years, but statistical studies of these data sets are only now beginning to be published [e.g., *Hofmann and Peterson*, 1998].

The U.S. Department of Energy's Atmospheric Radiation Measurement (ARM) program established the Southern Great Plains (SGP) Cloud and Radiation Testbed (CART) site in 1992 as the first of its field measurement sites [*Stokes and Schwartz*, 1994]. The CART site covers an area of ~142,000 km^2 in north central Oklahoma and south central Kansas and was designed to conduct measurements of radiation, cloud, and aerosol properties over a region similar in size to a satellite viewing area. It was chosen to represent a typical rural, midcontinental site, where satellite retrievals of atmospheric parameters are complicated by land use patterns. The SGP site consists of numerous heavily instrumented facilities capable of making in situ and remote-sensing observations of the atmosphere spread over the extent of the measurement area. It is distant from any large urban areas, so that the atmos-

Paper number 2001JD000785.

pheric aerosols over the site can often be interpreted as representative of mixed regional aerosols, although some large point source emissions, notably oil refineries and power plants, may impact the site from time to time. Also, local aerosol sources, including field-burning episodes and vehicular traffic, periodically affect the surface aerosol measurements.

The extent to which surface aerosol measurements represent the overlying atmospheric column is currently not well understood. Surface sites have the advantage of being able to be operated continuously over long periods and can show long-term trends and seasonal cycles in aerosol properties. It is important, however, to conduct studies of the vertical distribution of aerosol properties over these sites to determine under what conditions or at what times the surface measurements are similar to the column average properties. An aircraft program to conduct vertical profiles over the SGP CART site was started in early 2000 and is scheduled to continue for several years [*Andrews et al.*, 2001].

In order to interpret the radiation measurements made at the SGP CART site the extent to which local and/or regional activities influence the aerosol burden at or over the site and how they may influence the radiation measurements must be determined. In this context, several questions need to be addressed. Do local/regional farming, transportation, and industrial activities influence the aerosol properties at SGP? Agricultural fires, which are seasonal in nature (but also can occur at any time of the year), are known to occur very near the SGP Central Facility (CF) near Lamont, Oklahoma, and throughout the CART site. Could the smoke from these fires be sufficient to influence column radiation measurements such as optical depth? Is there a noticeable pattern to the emissions (presumably mostly sulfate) from the large oil refineries and power plants near the site (40–50 km away in Ponca City and Enid)? It is beyond the scope of this paper to provide definitive answers to all of these questions, but the aerosol measurements, when used along with other surface and column measurements at the site, can be useful in determining the impact local activities have on atmospheric radiative properties.

In this paper, we present the initial 4-year record of surface aerosol measurements from the Aerosol Observing System (AOS) at the Southern Great Plains CART site. The SGP AOS has been operational since July 1996, but significant system changes were made in early 1997 that permitted the determination of additional aerosol properties. In this paper, we report on surface aerosol observations at the site between the beginning of July 1996 and the end of June 2000. Our major objectives in this paper are (1) to provide details on the type and availability of surface aerosol measurements now being made continuously at the SGP CART site to the scientific user community, (2) to identify any daily, weekly, or seasonal variability or yearly trends that are evident in the surface aerosol data over the first 4 years of AOS operation, and (3) to report on the first year of aerosol hygroscopic growth measurements made at the SGP site.

2. Aerosol Observing System

2.1. Sample Air Inlet System

The AOS is housed in a fixed-location, temperature-controlled trailer (location: 36°36′19.6″N, 97°29′20.7″W, 315 m above sea level) at the SGP CF. Because of agricultural activities near the site, aerosol samples are obtained from the top of a stainless steel intake stack (~21.4-cm inner diameter) at a height of ~10 m above ground level. The stack is fitted with a rain cap, and sampling occurs from the underside of the cap through a metal screen designed to keep birds and insects from entering the system. Airflow through the stack is ~1000 L min^{-1}, and is divided into two separate flows. The sample flow (~150 L min^{-1}) is taken from the center of the stack tube and directed through a smaller stainless steel tube (4.75-cm inner diameter), where the aerosol is gently heated when necessary to achieve a low relative humidity (RH) of 40% or below. The sample flow then enters five sampling lines inside a manifold and is directed to the individual instruments. The flow in each sampling line (nominal 1.6-cm inner diameter) is controlled to 30 L min^{-1} either by critical orifices or mass flow controllers. The remainder of the stack flow is a sheath flow that passes the entrance to the sample flow tube and is exhausted through a blower and high-efficiency filter below the trailer.

When reporting the results of atmospheric aerosol measurements, it is important to discuss potential aerosol losses through the inlet system. Aerosol losses in inlets can be due to gravitational settling, diffusion to the walls, inertial deposition in tubing bends, turbulent deposition, and anisokinetic sampling issues. The gravitational settling velocity for 10-μm diameter particles (the largest particles permitted to enter our instruments) is ~0.3 cm s^{-1}, well over 2 orders of magnitude lower than the smallest flow velocity of ~46 cm s^{-1} in our inlet system. At the minimum flow velocity, only particles smaller than 3 nm are lost by diffusion to the walls with any significance, and these particles are not optically important and are not sensed by our particle counters. The stopping distance for 10-μm and 1-μm particles in our smallest tubing (~1.6-cm diameter) is <0.1 cm and ~0.01 cm, respectively, so that virtually all of even the largest sampled particles should be able to pass through the gentle bends in our sample lines. Turbulent deposition was calculated using the equations of *Friedlander*, [1977, Chapter 4]. The relatively low Reynolds numbers (~2600 to ~6400) and large tube diameters in our aerosol inlet system contribute to negligible turbulent deposition aerosol losses in the stack and 4.75-cm intake tube and losses of only a few percent for 10-μm particles in the 1.6-cm diameter tubing. While we have not measured the uniformity of the aerosol concentration for different particle sizes across the intake stack, the calculations presented above support a relatively uniform particle concentration. Certainly, sampling from the center of the stack (the subsampling point) minimizes wall loss concerns, which should increase approaching the viscous sublayer near the wall. At the subsampling point, where air from the center of the 21.4-cm stack enters the 4.75-cm tube, anisokinetic sampling losses are estimated at ~3% for 10-μm particles and <1% for 1-μm particles. In aggregate, losses for 10-μm diameter particles in our inlet system from all loss mechanisms are estimated to be <10%, and losses of particles between the diameters of 0.01 and 1 μm are believed to be well below 5%.

2.2. Instruments and Measurements

A switched impactor system was installed in March 1997 and provides for size-segregated aerosol light scattering and absorption measurements. Through the use of an upstream impactor, the instruments measuring aerosol light scattering and absorption always sample particles smaller than 10-μm aerodynamic diameter. Every 6 min a solenoid valve is opened or closed, and when closed, the sample aerosol is diverted through a 1-μm aerodynamic diameter cutpoint, multiple orifice impactor. In this way, alternating 1-μm (D_p < 1 μm) and 10-μm (D_p < 10 μm) size cuts are achieved.

The AOS comprises a set of instruments designed primarily for measuring aerosol microphysical and optical properties. Figure 1 shows a schematic of the AOS depicting the stack, manifold, sampling lines, and instruments. A condensation nucleus counter (CNC, TSI Model 3010) was used to measure the concentration of particles between ~0.01 and 3 μm in diameter. An optical particle counter (OPC, Particle Measuring Systems Model PCASP-X) provided size distribution data in 31 size channels for particle sizes between 0.1 and 10 μm. The OPC data presented in this paper are the number concentration of particles detected over the entire OPC size range. When combined with the CNC data, the OPC measurements provide an estimate of the fraction of all particles that are optically important in the visible wavelengths. The aerosol light absorption coefficient (σ_{ap}) was measured using a filter-based light

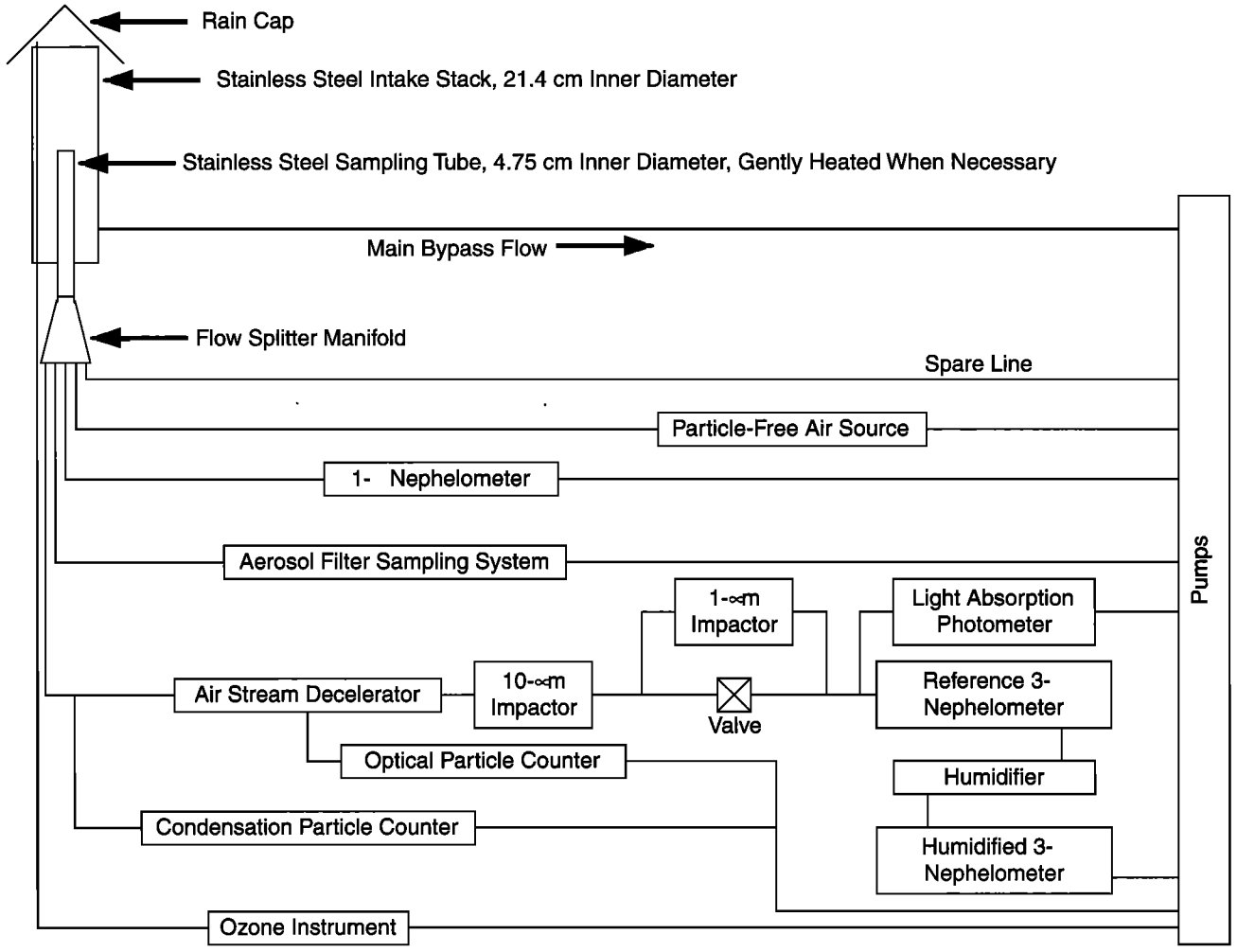

Figure 1. Schematic of the Aerosol Observing System (AOS) at the ARM Southern Great Plains CART Central Facility.

absorption photometer (Radiance Research Model PSAP), which was calibrated to estimate suspended-state aerosol light absorption at 550 nm using an extinction cell and a nephelometer [*Bond et al.*, 1999]. Two independent nephelometer-based systems measure light scattering by aerosol particles. A single-wavelength nephelometer (Radiance Research Model M903) measures σ_{sp} at 545 nm. The single-wavelength measurements will not be discussed in this paper. A second system consisting of two nephelometers (TSI Model 3563) [*Anderson et al.*, 1996; *Anderson and Ogren*, 1998] and a humidifier (called a humidograph) measures σ_{sp} as a function of RH at three visible wavelengths (nominally 450, 550, and 700 nm) and over two ranges of angular integration (7–170° and 90–170°). The two nephelometers are connected in series separated by the humidity control system that is programmed to ramp the RH in the second nephelometer over a 1-hour period between ~40 and 90%. This scanning humidograph was modeled after and operated in a manner similar to that described by *Carrico et al.* [1998], except that the humidity was ramped to slightly higher values in this study. Because the two nephelometers measure σ_{sp} at different RHs, an estimate of the σ_{sp} at ambient or any other RH ($\sigma_{sp(RH)}$) over the duration of the RH scan period can be made through the use of a three-parameter curve-fitting model similar to that described by *Kotchenruther and Hobbs* [1998]:

$$\sigma_{sp(RH)}/\sigma_{sp(RH=40\%)} = a[1 + b(RH/100)^c], \quad (1)$$

where a, b, and c are the calculated fit parameters and $\sigma_{sp(RH=40\%)}$ is calculated by adjusting the low-RH σ_{sp} measurement to 40% RH using the fit parameters. The humidograph system permits the determination of the aerosol hygroscopic growth factor, $f(RH)$, which has been defined as the change in aerosol light scattering with changing RH [*Covert et al.*, 1972; *Rood et al.*, 1987]. For this paper, $f(RH)$ was defined as

$$f(RH) = \sigma_{sp(RH=85\%)}/\sigma_{sp(RH=40\%)} \quad (2)$$

and was calculated using (1) with the scattering coefficient values adjusted to 40% and 85% RH. While one of the three-wavelength nephelometers has been in operation since the beginning of the aerosol data record, the complete humidograph system was not installed until December 1998. Therefore we present hygroscopic growth data only for 1999. An aerosol filter sampling system was added in early 2000 to collect particles for subsequent physical and chemical (i.e., gravimetric mass, ion chromatography) analysis. Ozone concentration was continuously measured using an ultraviolet photometric ozone analyzer (Dasibi Model 1008-RS). Neither the ozone measurements nor the few chemical filter analyses performed as of early 2000 will be discussed in this paper.

Table 1 provides a summary of all AOS instruments and measurements, along with equations for the derived aerosol radiative properties. Of these instruments the three-wavelength nephelometer and the light absorption photometer provide critical measurements for the calculation of direct aerosol radiative forcing. The σ_{sp} and σ_{ap} measurements reported in this paper have units of inverse megameters (Mm^{-1}, or 10^{-6} m^{-1}). The aerosol single-scattering albedo ω_0 at the 550-nm wavelength is

Table 1. Instruments and Atmospheric Measurements Made at the ARM/SGP AOS

Instrument	Primary Measurements	Derived Measurements
TSI Model 3563 three-wavelength, backscatter/total scatter integrating nephelometers, operated at both low (<40%) and variable (~40–90%) relative humidity	total scattering and hemispheric backscattering coefficients (σ_{sp} and σ_{bsp}) from $D_p < 1$ μm and $D_p < 10$ μm particles at 450, 550, and 700 nm	hemispheric backscatter fraction, $b = \sigma_{bsp}/\sigma_{sp}$ Ångström exponents, $\mathring{a} = -\log[\sigma_{sp}(\lambda_1)/\sigma_{sp}(\lambda_2)]/\log[\lambda_1/\lambda_2]$ single scattering albedo, $\omega_0 = \sigma_{sp}/(\sigma_{sp} + \sigma_{ap})$ submicrometer scattering fraction, $R_{sp} = \sigma_{sp\ (1\text{-}\mu m)}/\sigma_{sp\ (10\text{-}\mu m)}$ at 550 nm hygroscopic growth factor, $f(RH) = \sigma_{sp(RH\ =\ 85\%)}/\sigma_{sp(RH\ =\ 40\%)}$
Radiance Research Model M903 single-wavelength integrating nephelometer	total scattering coefficients from particles, σ_{sp}, at 545 nm	
Radiance Research Model PSAP particulate light absorption photometer	light absorption coefficient (σ_{ap}) from $D_p < 1$ μm and $D_p < 10$ μm particles, at 550 nm[a]	single scattering albedo, ω_0, at 550 nm
TSI Model 3010 condensation nucleus counter	total particle concentration over the range 0.01–3 μm diameter	none
Particle Measuring Systems Model PCASP-X optical particle spectrometer	particle concentration in each of 31 size ranges between 0.1 and 10 μm	particle size distributions (number, surface area, volume, mass)
Dasibi Model 1008-RS ozone monitor	ozone mixing ratio	none

[a] PSAP instrument uses 565 nm incident radiation to determine the absorption coefficient. These data are corrected to 550 nm through the use of the calibrations given by *Bond et al.* [1999].

derived from measurements of σ_{sp} at that wavelength and σ_{ap} adjusted to 550 nm using the calibrations reported by *Bond et al.* [1999]. The hemispheric backscatter fraction b is used to estimate β; the relationship between the two was originally derived by *Wiscombe and Grams* [1976]. The Ångström exponent $\mathring{a}$ is estimated in this paper using 550- and 700-nm aerosol scattering data. The humidified σ_{sp} measurements provide a way to convert scattering measurements taken at instrument RH to ambient conditions. The submicrometer scattering ratio R_{sp}, defined as $\sigma_{sp\ (Dp\ <\ 1\ \mu m)}/\sigma_{sp\ (Dp\ <\ 10\ \mu m)}$ at 550 nm, permits apportionment of light scattering into submicrometer and supermicrometer aerosol modes.

Instrument control and monitoring, calibrations, zero checks, and data acquisition are all performed through a dedicated computer workstation. The computer continuously monitors high-frequency aerosol measurements and then calculates and archives 1-min average data. The AOS computer is connected to the SGP Site Data System via a fiber optic link from the aerosol trailer to the control trailer. In this paper, the 1-min AOS aerosol data have been processed with longer averaging times for the purpose of calculating hourly, daily, and monthly statistics and determining variability over longer timescales.

2.3. Calibrations, Corrections, and Uncertainties

The calibrations of the TSI 3563 nephelometers are checked weekly by filling the instruments with particle-free gases of known scattering coefficients. These span gas checks, which are performed with air and CO_2, typically show that scattering at the three wavelengths is within a few percent of the expected values. The major correction that must be applied to the TSI nephelometer measurements is for angular nonidealities. The total scattering and hemispheric backscattering coefficients are measured over integration angles of ~7–170° and 90–170°, respectively, and these must be corrected to the full 0–180° and 90–180° ranges. A size-dependent truncation correction based on the Ångström exponent has been applied [*Anderson and Ogren*, 1998].

Calibration of the PSAP is performed as described by *Bond et al.* [1999], who used a reference suspended-state absorption determined as the difference between the measurements from a light extinction cell and a nephelometer. This calibration takes into account a spot size correction, an adjustment of the σ_{ap} from 565 nm (the wavelength used in the PSAP) to 550 nm, and a correction for filter-based scattering that is sensed as absorption by the instrument.

Calibrations of the OPC occur whenever the need arises but not less frequently than once per year. Calibration involves cleaning the optics, aligning the laser, maximizing the sensed counts, and adjusting the gain ranges so that standard particles of known sizes are sensed in the correct channels. We continuously monitor the laser reference voltage, and low laser voltages generally signal that a routine service for the OPC is due.

The CNC is calibrated against our laboratory standard particle counter approximately once per year. While not an absolute calibration, it is a necessary consistency check. The count rate of the CNC is tuned by cleaning the optical and other internal surfaces of the unit and then checking the pulse characteristics from the sensed particles against manufacturer specifications. The volumetric flow rate through the CNC is calibrated using a volumetric flow calibration unit, and the critical orifice is cleaned several times per year to ensure an accurate flow rate.

Uncertainties for the TSI 3563 nephelometer measurements have been described in detail by *Anderson and Ogren* [1998]. Calculation of the measurement uncertainty associated with the nephelometers can be calculated from four major sources and is expressed as a linear combination of the following terms:

$$\delta\sigma^2_{total} = \delta\sigma^2_{noise} + \delta\sigma^2_{drift} + \delta\sigma^2_{cal} + \delta\sigma^2_{trunc}, \quad (3)$$

where $\delta\sigma_p$ designates the uncertainty in σ_{sp} associated with the parameter P (at a 95% confidence level). These individual uncertainties are instrument-specific and represent (1) instrumental noise (~7% at $\sigma_{sp} = 33$ Mm^{-1}), (2) drift in the calibration based on repeated measurements of calibration gases (4%), (3) uncertainty in the calibrations due to uncertainties in the measured Rayleigh scattering of air and CO_2 (5.5%), and (4) uncertainty in the truncation or blocking of near-forward scattered light (2%). At the median reference nephelometer (low RH) scattering values observed in this study (~33 Mm^{-1}) the total analytical uncertainty from all sources in the 1-min average σ_{sp} measurements is ~10%.

Uncertainty in the PSAP-derived σ_{ap} results from uncertainty in the following components of the measurement: (1) instrument accuracy (~20%), (2) instrument precision (~6%), (3) instrument

noise (fixed at 0.88 Mm^{-1} for a 1-min averaging time), and (4) uncertainty in the *Bond et al.* [1999] calibration that converts the wavelength to 550 nm and corrects for filter-based scattering that is sensed as absorption by the instrument (~4%). Added in quadrature as in equation (3), these components yield total uncertainties in the 1-min average data of $\delta\sigma_{ap}$ ~49% for $\sigma_{ap} = 2$ Mm^{-1} and $\delta\sigma_{ap}$ ~28% for $\sigma_{ap} = 5$ Mm^{-1}. While these uncertainties in the σ_{ap} measurement are quite large, they are representative of the current state of the art in filter-based light absorption measurements.

Uncertainties in the CNC measurements arise from uncertainties in the sample flow rate (~10%, held constant by a critical orifice), the ~50% counting efficiency at the lower size limit of detection (0.01-μm diameter), and the <10% coincidence counts at a particle concentration of 10,000 cm^{-3}. We have not attempted to correct the condensation nucleus (CN) counts for the low counting efficiency at very small particle sizes, nor have we addressed coincidence errors. Therefore CN counts should probably be viewed as lower limits to the true concentration of particles larger than 0.01 μm.

The OPC measurements have uncertainties associated with them due to uncertainties in the sample flow rate (~2%), sizing uncertainties due to oscillations in the scattering response curve and due to unknown particle refractive index and morphology, and uncertainties in the correction of a counting efficiency of ~50% at the lowest size channel increasing to 100% by the fourth size channel. Sizing uncertainties resulting from oscillations in the scattering response curve and for counting efficiency in the smallest size ranges are difficult to quantify but are not considered to be major uncertainties by the manufacturer. Coincident particle counting is not considered a problem given the moderate particle concentrations typically observed at the SGP site. The refractive index makes little difference in sizing below ~0.8 μm diameter, unless the aerosol is heavily absorbing. Above ~0.8 μm, if one assumes an intermediate value of 1.44 for the real component of the refractive index, this uncertainty introduces a sizing error of up to ~25% (depending on the size of the particle) from the sizes determined by calibration with polystyrene latex (PSL) microspheres [*Kim*, 1995]. Since the AOS OPC is calibrated using PSL microspheres, the reported size range should be viewed as a PSL equivalent size range. Since the OPC data presented in this paper represent the number concentration of particles detected over the entire OPC size range, and since the lower limit size of ~0.1 μm does not change appreciably due to refractive index uncertainties, the minimal correction necessary to convert to ambient particle sizes was not attempted. Because of the wide collection angles used in the PCASP-X, asphericity has little effect on particle sizing, probably <5%.

3. Results and Discussion

3.1. Four-Year Time Series

Four-year time series of daily average aerosol data for some important AOS aerosol parameters are shown in Figure 2. Linear least squares fits have been performed on the data, and the fit line has been added to each plot to show data trends. With the exception of the CNC and OPC measurements, aerosols were passed through a 10-μm-diameter cutpoint impactor to remove the largest particles. These very large particles typically comprise a minuscule fraction of the aerosol number density except during the relatively infrequent dust or fog episodes at the site, so their exclusion usually did not influence the ambient size distribution. Gaps in the data records are due to several factors. Instrument failures or other operational problems associated with each instrument accounted for some of the observed gaps. Problems with microprocessor control of the electronically actuated ball valve that switched the system size cut from 1 to 10 μm were responsible for other gaps. In about half of those cases the system was held at the 1-μm cutpoint, so that submicrometer AOP data exist but are not shown on the D_p < 10-μm aerosol plots. The period before March 1997 was before the impactor-switching valve was installed, so R_{sp} was not measured during these times. Finally, a system leak was discovered and repaired in mid-1998 that affected measurements in some sampling lines.

It should be noted that the data set has been manually edited to remove invalid data resulting from instrumental or sampling problems. A computer algorithm has also been used to screen for anomalous data. Once identified, anomalous data are then investigated to determine if they should be removed from the data set. Data from infrequent very low scattering and absorption episodes have been retained, even though there may be a significant influence from instrument noise at these levels. Calculation of ω_0, b, $\mathring{a}$, and R_{sp} during these low-aerosol episodes produces noise-influenced values and occasionally generates values that are unrealistic (e.g., ω_0 values >1.0). Fortunately, these data occur very infrequently in the data record, and their inclusion does not significantly change the reported average values or the conclusions of this paper.

The OPC-derived particle concentrations from late 1998 through the middle of 1999 appear lower than normal. The instrument was serviced during this time, and no cause for the lower count rate was identified. Other aerosol parameters during this interval generally showed average to below-average values (much of this occurred when the cut size was held at 1 μm, so the other aerosol data are not plotted) but not markedly lower values. We have marked these data as "questionable" in the ARM data archive but have not eliminated them without definitive evidence of a problem. The trend line is clearly heading downward, but it is heavily influenced by the questionable data period in the second half of the data record.

While the daily average time series data often showed considerable variability over relatively short timescales (e.g., 2–3 days), some parameters varied dramatically over the period of a few hours. For example, hourly average CNC concentrations sometimes varied by a factor of 3 or more over the course of the day, with lower values in the early morning and highest values in late afternoon. Similarly, when smoke plumes from local agricultural burning were sampled, large spikes in the absorption coefficient (a factor of 10 or more higher than the previous values), which lasted typically from one to several hours, were observed. The statistical variability of these data over other timescales is discussed in section 3.2.

Typical values of the daily average σ_{ap} are near or below a few Mm^{-1} over most of the 4-year period. Many peaks in the record correspond to field- and ditch-burning episodes by local farmers near the site. There is a broad peak in the absorption record in May 1998 that has been attributed to Central American smoke aerosols reaching the CART site [*Peppler et al.*, 2000]. In 1999 the variability and the magnitude of the absorption coefficient appear to have increased, which may reflect an increased frequency of biomass and/or fossil fuel combustion (e.g., local burning episodes, vehicular traffic) near the site over the previous 2 years. Single-scattering albedo also appears to be dropping slightly with time, a direct consequence of the increase in absorption coefficient with no significant corresponding increase in the scattering coefficient. During the second half of 1999 our measurements indicate an increased prevalence of high absorption (i.e., $\sigma_{ap} > 5$ Mm^{-1}) episodes at the SGP CF. The single-scattering albedo plot clearly shows an abundance of low values ($\omega_0 < 0.85$, corresponding to darker aerosols) at this time. A linear least squares fit of the data shows the σ_{ap} to have increased at a rate of ~0.5 Mm^{-1} yr^{-1} and the ω_0 to have decreased by ~0.016 (1–2%) yr^{-1} since the middle of 1996. These trends are, necessarily, based on relatively short time series, and more measurements are necessary to verify any long-term trends. The median ω_0 value for the period September 1 to December 31, 1999, was 0.88, compared with the 4-year median of 0.95 and the 1999 median of 0.91. Sixty-two percent of the hourly observations of ω_0 during the last 4 months of 1999 were lower than 0.9, while 26% were lower than 0.85.

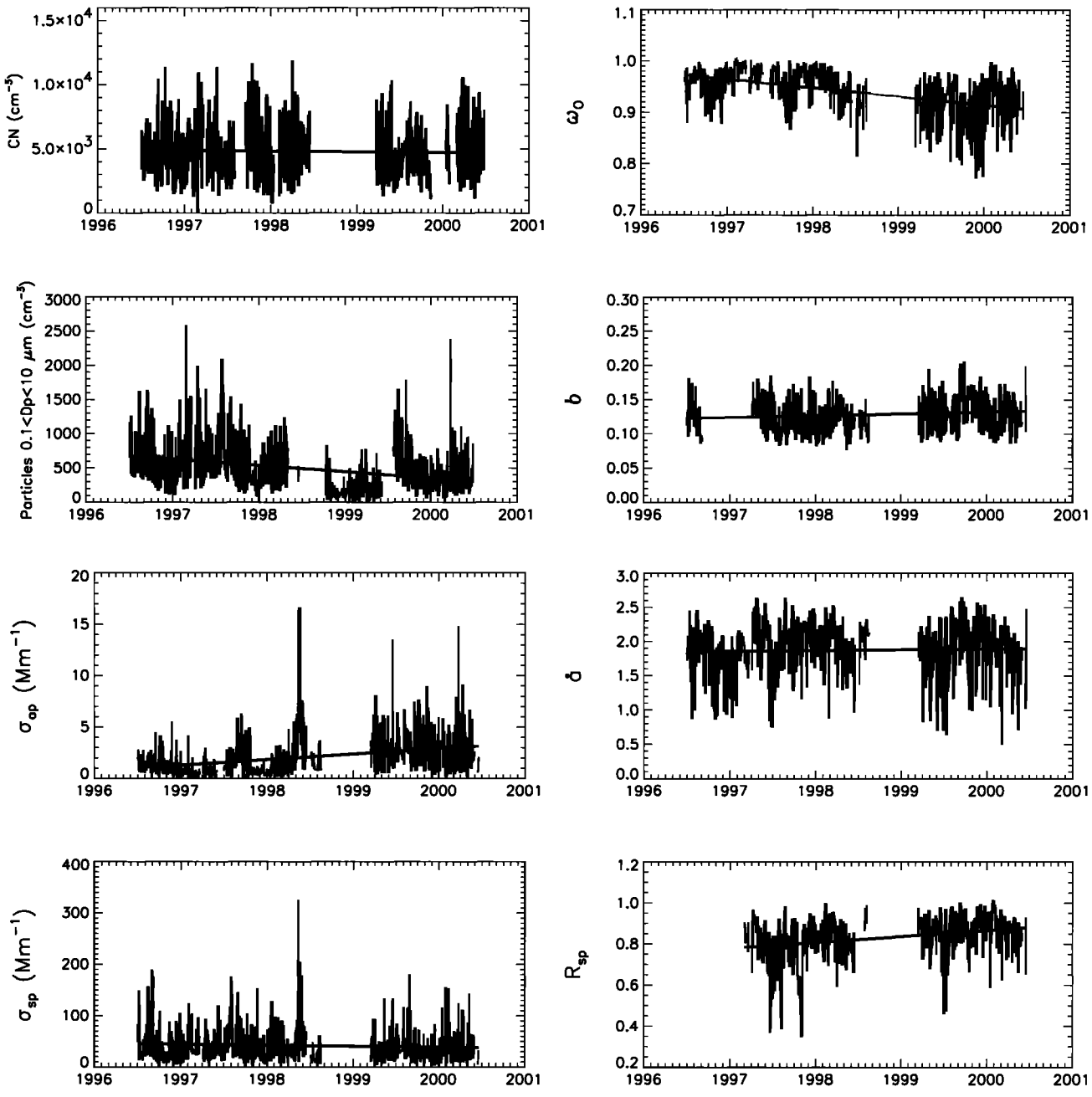

Figure 2. Four-year time series of daily average, D_p < 10 μm aerosol data at the SGP CART site. Trend lines, representing least squares fits of the data, are shown.

This autumn decrease in ω_0 is also evident in the data from 1996 and 1997, although it is not as striking as the 1999 event. Instrument problems during late 1998 precluded obtaining ω_0 measurements at that time. In early March 2000 a very brief but intense burning episode very close to the SGP CF caused the daily average σ_{ap} at the site to reach 15 Mm^{-1}, while the hourly average σ_{ap} exceeded 100 Mm^{-1}. Overall, the first half of 2000 has shown higher ω_0 values than those of late 1999.

Daily average measurements of R_{sp} were lower for much of 1997 than at most times thereafter. Two extended periods and one brief period of low-R_{sp} measurements are clearly visible during 1997. The first of these, which occurred around late June, appears to coincide with a dip in *å*, which would also suggest that larger particles were being sampled at this time. Over the study period the submicrometer scattering ratio increased at a rate of ~3% yr^{-1}, although if the two low-R_{sp} periods in 1997 are removed, the trend drops to <1%.

With the exception of *b*, which shows a very slight increase with time, the other plotted AOPs show considerable variability but no obvious trends over the 4-year period. The major peak in σ_{sp} at the beginning of August 1997 is due to a local field-burning episode, which is also apparent in the σ_{ap} record. The May 1998 scattering peak from the Mexican fires is also evident in these data and is the dominant feature in the scattering coefficient record.

3.2. Daily, Weekly, and Annual Aerosol Cycles

Surface aerosol data from the AOS have been grouped by hour of the day, day of the week, and month of the year and analyzed to determine daily, weekly, and annual characteristics and cycles. Distributions of hourly average, D_p < 10 μm aerosol data, repre-

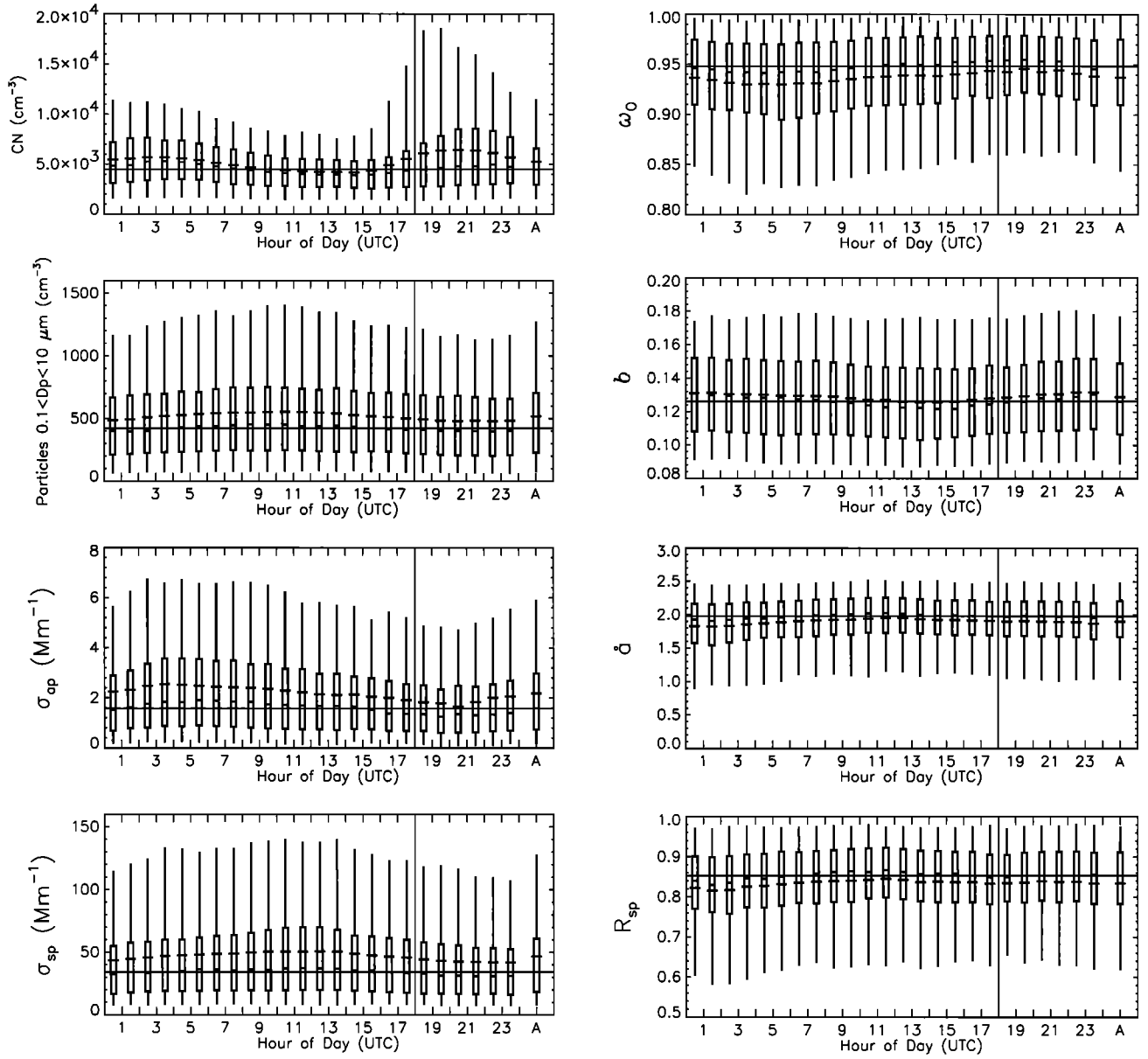

Figure 3. Statistical analysis showing hourly average, $D_p < 10$ μm aerosol distribution data over the 4-year period sorted by hour of the day. The ends of the boxes, the ends of the whiskers, and the shorter line across each box represent the 25th and 75th percentiles, the 5th and 95th percentiles, and the median, respectively. The mean is represented by the longer line with ends extending well beyond the sides of the box. The distribution at the far right of each plot represents all hourly data, and the median line for that distribution is drawn across the entire plot. The vertical line at 1800 universal time coordinated (UTC) is for local noon (1200 LT).

sented as box-and-whiskers plots and grouped by hour, are shown in Figure 3. In each plot in this section, the ends of each box represent the 25th and 75th percentiles of the distribution, the ends of the whiskers represent the 5th and 95th percentiles, and the shorter line across the box is the median of the distribution. The mean is represented by the longer line with ends extending well beyond the sides of the box. Data from the 24 hours in each day are shown along with a final box showing the cumulative statistics for all hours. The horizontal line extending across all distributions is the median for all hourly data. The vertical line at 1800 universal time coordinated (UTC) represents local noon (1200 LT). It is interesting to note that very similar multiyear, daily aerosol cycles described below were observed at our other continental U.S. aerosol monitoring site (Bondville, Illinois), although the cycles were typically more pronounced there than at the SGP site (D. J. Delene and J. A. Ogren, Variability of aerosol optical properties at four North American surface monitoring sites, submitted to *Journal of Geophysical Research*, 2001; hereinafter referred to as Delene and Ogren, submitted manuscript, 2001). The strongest daily cycle is observed in the CNC data. Condensation nucleus (CN) counts are lowest during the hours of 0900–1600 UTC. Because the site is 5 or 6 hours behind UTC depending whether or not daylight savings time is in effect, this corresponds to 0400–1100 LT during the summer. Median CN counts begin to rise at about 1600 UTC and remain elevated until the next day, when they start to decrease to their minimum values near 0900 UTC. The cycle is even more pronounced when looking at the 75th and 95th percentile populations. The 75th percentile distribution peaks between 2000 and 2200 UTC, and the 95th percentile distribution peaks at 1900–2000 UTC (both are mid- to late-afternoon local time). This indicates that the dramatic afternoon increases in CN counts were present perhaps 25% of the time. The CN data show a

similar daily cycle for individual years as for the 4-year period. This afternoon CN peak can be found at any time of the year, but the highest CN concentrations on high-CN days appear during summer to early autumn. Possible explanations for the high afternoon CN levels include sulfate formation from SO_2 emissions from local power plants or refineries, photochemically driven production of organic or N-containing particles, and/or diurnal convective mixing and stability cycles. At this time, there are insufficient chemical filter data to support or reject any of these possibilities, and the true explanation might be a combination of all these factors.

To determine whether the differences observed in the hourly CN distributions are statistically significant, we used Mann-Whitney tests. This test is similar to an independent group t test, except that no assumptions of normality or equality of variance are made, and it uses the ranks of the data rather than their raw values to calculate the probability statistic. Since the means are not compared, we cannot say whether or not the means are significantly different. In the following comparisons we have stated whether or not differences in the compared distributions are significant at a given confidence level.

For the hourly distributions of CN counts we chose an hour in the minimum portion of the cycle (hour 13) and compared it with all other hours in the cycle. At a confidence level of 95% the distributions for all hours except hours 10, 11, 12, 14, 15, and 16 were statistically different from that of hour 13. This indicates that the large rise in CN counts during the local afternoon hours is statistically significant.

A similar result was obtained for the hourly distributions of most parameters. Since the distributions appear to change gradually over the hours, differences in the distributions of hours that were either adjacent or separated by only a few hours were usually not statistically significant. Statistical differences between hours from maximum and minimum parts of the daily cycles almost always were significant at the 95% confidence level.

The daily cycles of summed hourly average OPC counts (all particles between 0.1 and 10 μm diameter) and σ_{sp} are similar, and both show a weak, broad peak near 1000 UTC (0500 LT during the summer). This agreement is to be expected since particles sensed by the OPC are in the correct size range to scatter visible light effectively in the nephelometer. The median σ_{sp} value (dry aerosols, 550 nm) for the SGP CART site over the 4-year period was $\sim$33 Mm^{-1}. These broad distributions peak between 1000 and 1200 UTC (depending on the population), and this corresponds to the early morning hours at the site. A possible explanation for these distributions is that rainfall at the site is more commonly observed in the afternoon and evening hours than in the early morning. Rainfall is effective at removing accumulation mode and larger particles from the atmosphere, and these later hours show values consistent with lower aerosol amounts. Vertical mixing may also be important in explaining the timing of the observed aerosol distributions.

The daily cycles of hourly average σ_{ap} and ω_0 are also quite similar to one another, although inversely related. The absorption coefficient appears to vary smoothly from its peak median around 0600 UTC to its minimum near 2000 UTC. Single-scattering albedo shows nearly the same cycle with the maximum and minimum reversed. This suggests that the ω_0 cycle is being driven more by the variability in σ_{ap} than the gradual hourly changes in σ_{sp}. The median σ_{ap} value (dry aerosols, 550 nm) for the study period was $\sim$1.5 Mm^{-1}, while the median ω_0 was $\sim$0.95. The hourly distributions of both σ_{ap} and ω_0 showed differences between the maximum and minimum portions of each one's daily cycle that were statistically significant at the 95% confidence level.

Distributions of hourly average, $D_p < 10$ μm aerosol data grouped by day of the week are shown in Figure 4. No strong weekly cycles were observed for any of the aerosol parameters, although the differences between the minimum and maximum portions of the cycles were usually statistically significant at the 95% confidence level. A midweek (Wednesday and Thursday) minimum in R_{sp} is observed, suggesting a greater fraction of larger particles at that time. The highest values of R_{sp} fall on the weekend. Weekly cycles for σ_{ap} and ω_0 are weak but present, with Sunday and Monday showing the lowest σ_{ap} and highest ω_0 median values. The Sunday and Monday distributions for both σ_{ap} and ω_0 are statistically different at the 95% confidence level from those of any other day of the week. CN counts were lowest on Sunday, and the difference between the Sunday distribution and that of any other day of the week was also statistically significant at 95% confidence. It is possible that reduced vehicular traffic or less agricultural burning in the area on the weekends could explain these observations.

Monthly distributions of hourly average, $D_p < 10$ μm AOS aerosol data are plotted in Figure 5. The CN median data do not show a single monthly maximum but rather show local maxima in March and October. In contrast, the summed OPC median data indicate a strong peak in larger particles in mid- to late summer. The monthly $\mathring{a}$, b, and R_{sp} median data all show dips in the midsummer, which generally support the OPC data and can be related to an increase in the fraction of larger particles during the midsummer. This may possibly be related to summertime wind-blown dust episodes caused by convective activity or frontal passage. There is a period showing elevated light absorption coefficients (all above the annual median) in the late spring through autumn (April through October). There are also generally lower ω_0 values over the same months, although the higher August value is mostly due to the August maximum in σ_{sp}. The strong October decrease in ω_0 over the 4-year period was observed in all years except 1998, when no $D_p < 10$ μm absorption data were collected. An even larger drop in ω_0 occurred in the late autumn and early winter of 1999, which suggests that the local agricultural burning season may have been extended that year.

The monthly data in Figure 5 show that over the 4-year period the major reduction in ω_0 occurs in October, with a lesser effect seen in September. November and December also show median values that are near or below the overall median, indicating that the low ω_0 values in November and December 1999 were not anomalous data. January and February show ω_0 median values well above the annual median, with the following months dropping to a secondary minimum in June. A similar autumn decrease in ω_0 has been observed at our rural Bondville, Illinois, aerosol station (Delene and Ogren, submitted manuscript, 2001) and may be related to synoptic-scale agricultural, transportation, or atmospheric flow patterns.

Most of the monthly distributions were significantly different at the 95% confidence level from any other monthly distribution for a given parameter. For example, σ_{ap} shows a broad maximum in the summer and fall months and a minimum in the winter. On average, each monthly distribution is statistically different (at the 95% confidence level) from 10 other monthly distributions. The maximum in the σ_{ap} annual cycle occurs in October, and that monthly distribution is statistically different from every other monthly distribution except August, including the months adjacent to October.

3.3. Aerosol Hygroscopic Growth

Measurements of the hygroscopic growth of aerosol particles have been made at the SGP CF site since December 1998. Figure 6 (top) shows the fitted f(RH) data for hourly average, $D_p < 10$ μm particles plotted as a time series for 1999. The time series data are calculated from all valid 1-min average observations of σ_{sp} (humidified and dry at 550 nm). Problems with the control of the impactor-switching valve caused only $D_p < 1$ μm data to be collected for the first 2 months of 1999. The hourly f(RH) values range from $\sim$1.0 to 3.3, with a median of 1.83. A box-and-whiskers plot showing the variability of the distribution of f(RH) values by hour for 1999 is shown in Figure 6 (bottom). The hourly medians increase starting at 1600 UTC up to a maximum at 2200

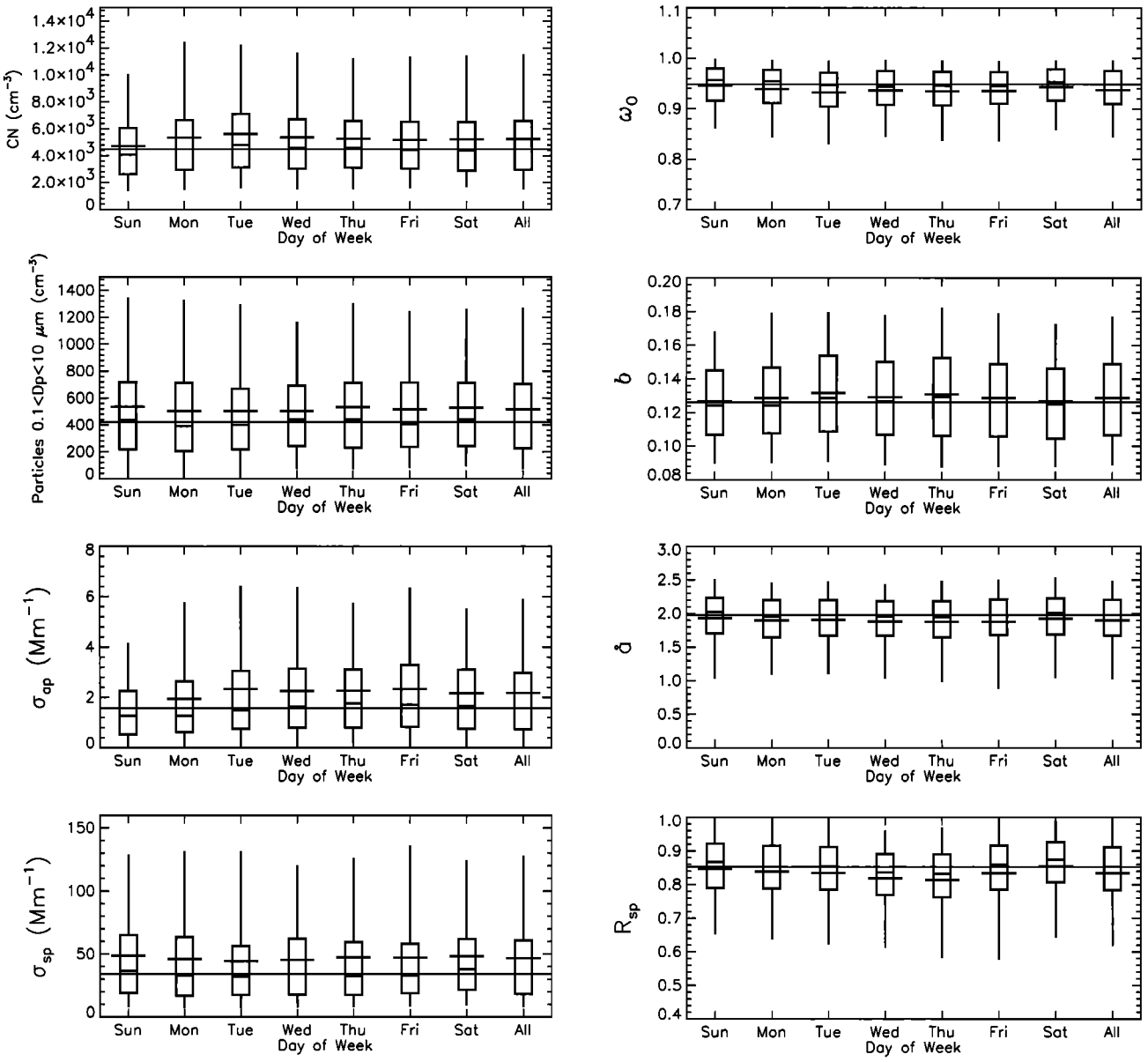

Figure 4. Statistical analysis showing hourly verage, $D_p < 10$ μm aerosol distribution data over the 4-year period sorted by day of the week. The ends of the box, the ends of the whiskers, and the shorter line across each box represent the 25th and 75th percentiles, the 5th and 95th percentiles, and the median, respectively. The mean is represented by the longer line with ends extending well beyond the sides of the box. The distribution at the far right of each plot represents all hourly data for the week, and the median line for that distribution is drawn across the entire plot.

UTC. This late afternoon increase corresponds with the concurrent increase in observed CN counts. It suggests that the particles associated with the afternoon increases in CN counts are more hygroscopic than those observed at other times. This behavior is consistent with CN counts being indicative of submicrometer aerosols and the supermicrometer aerosols being predominantly mineral dust, although chemical or other measurements are necessary to confirm the dust hypothesis.

Frequency distributions of the aerosol hygroscopic growth data from SGP are shown in Figure 7. Data points are plotted as the midpoint of each data bin, and bins are 0.1 f(RH) units wide. The number of valid RH scans in 1999 used in the compilations for $D_p < 10$ μm and $D_p < 1$ μm particles exceeds 5000 for each size range and is shown in the legend. Figure 7 shows that the frequency distributions of f(RH) for $D_p < 1$ μm and $D_p < 10$ μm particles are very similar. The spread of observations for the two size ranges is nearly identical, and the peaks in the two distributions are within ~0.1 of one another, with that of the $D_p < 1$ μm size fraction falling just below that of the $D_p < 10$ μm aerosols. At higher values of f(RH), the smaller size fraction shows a higher frequency of observations, and the median of this population is slightly higher at 1.86. Analysis of time series plots of the two size ranges show that the f(RH)values for $D_p < 1$ μm particles are usually larger than for $D_p < 10$ μm particles for concurrent observations when the f(RH)is above ~2. If a significant fraction of the smaller aerosol particulates are composed mostly of sulfate and the $D_p < 10$ μm aerosol has soil dust and possibly other hydrophobic material mixed in, then this size dependence in f(RH)would be expected.

An attempt was made to characterize the conditions that led to very high and very low values of f(RH). We have sometimes observed f(RH) to increase concurrently with the afternoon increase in CN counts. More study needs to be done on the

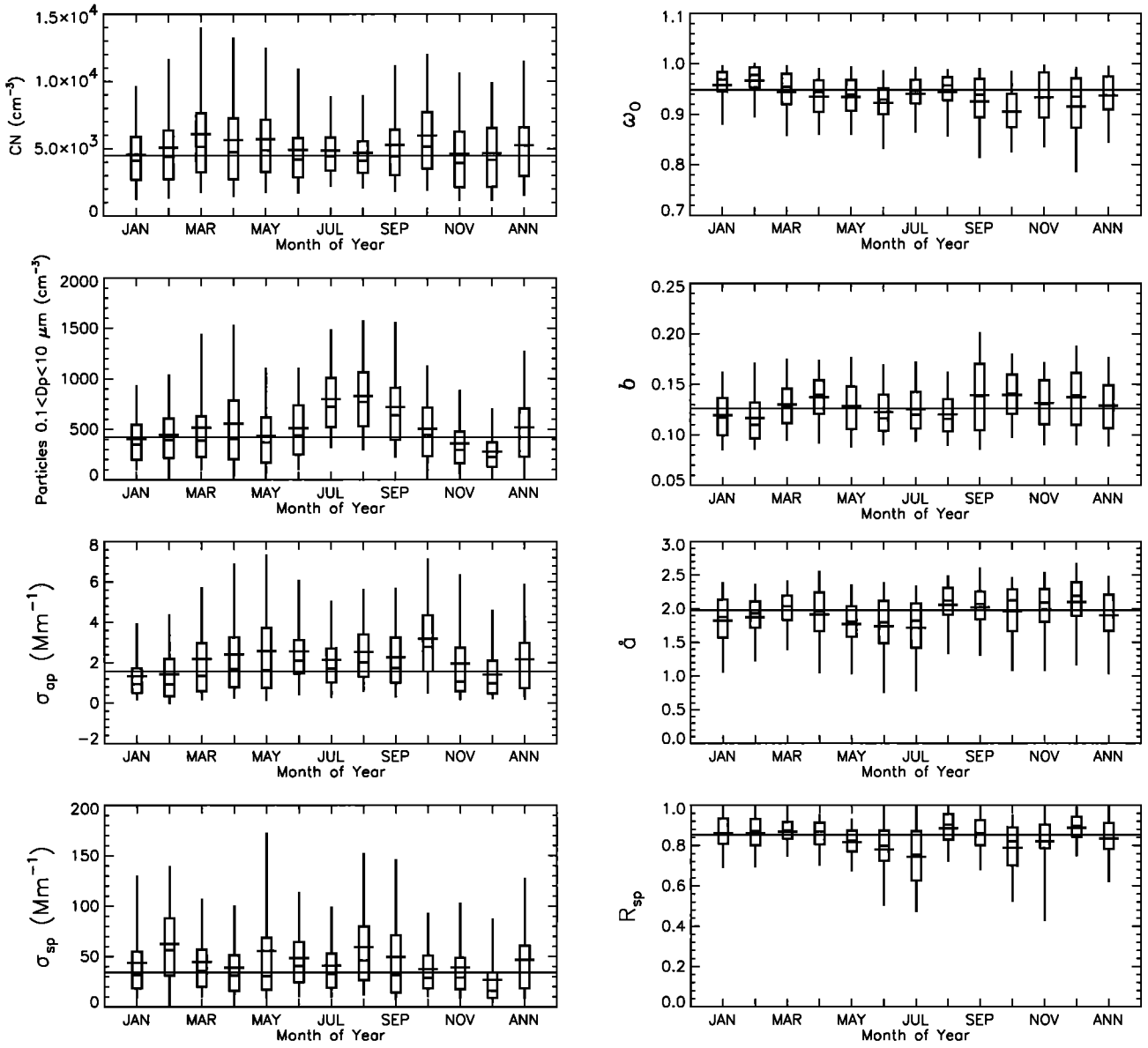

Figure 5. Statistical analysis showing hourly average, $D_p < 10$ μm aerosol distribution data over the 4-year period sorted by month of the year. The ends of the box, the ends of the whiskers, and the shorter line across each box represent the 25th and 75th percentiles, the 5th and 95th percentiles, and the median, respectively. The mean is represented by the longer line with ends extending well beyond the sides of the box. The distribution at the far right of each plot represents all hourly data for the year, and the median line for that distribution is drawn across the entire plot.

meteorological conditions present when these afternoon increases are observed and also on the aerosol chemistry for days with these conditions. Without these additional analyses it would be difficult to unambiguously classify the aerosol type(s) causing these increases.

Low-f(RH) measurements identify periods when the aerosol was less hygroscopic. Several papers in the recent literature have related low-f(RH) measurements to Saharan dust [*Li-Jones et al.*, 1998; *Gassó et al.*, 2000] or biomass smoke [*Kotchenruther and Hobbs*, 1998] aerosols. Both dust from fields during windy periods and smoke from the burning of agricultural fields and roadside ditches are commonly observed in the vicinity of the SGP CF. Local farmers frequently use fire as part of their management scheme, in a manner suited to their particular cropping requirements. Because there are several different local crops that are harvested at different times and because roadside ditch and unused field burning can occur at any time of the year, the smoke from these fires is not strictly a seasonal phenomenon but is generated in varying amounts over most of the year.

During one 10-day maintenance visit to the SGP CF in July 1999 we observed a large number of field fires in close proximity to the site. Fires were as close as several hundred meters away in the next field. Unfortunately, our instruments were shut down at this time, and no AOP data were collected. The meteorological logs over this period show that at least 43 hourly observations were made with some mention of smoke from field fires. There were undoubtedly more hours influenced by smoke than this because some smoke observations were apparently not entered into the log files by the observers and visual observations of the smoke are not made at night. Possibly, only the closest fires that could potentially influence the vertical measurements were documented in the log files, whereas smoke from greater distances (and not apparent to the meteorological observer) can influence the surface aerosol measurements [e.g., *Peppler et al.*, 2000].

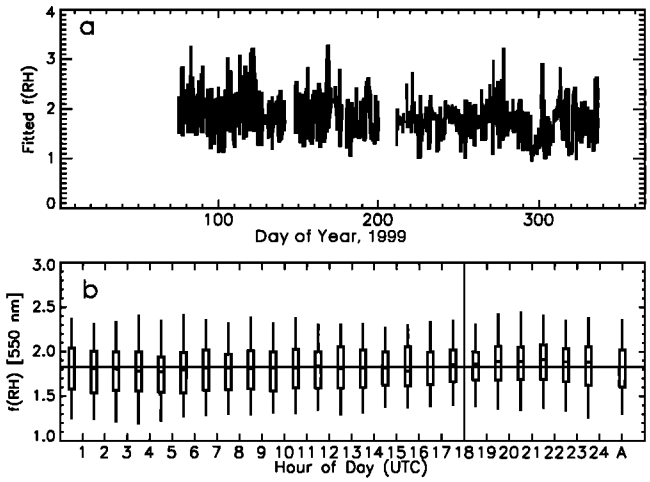

Figure 6. (top) One-year time series showing hourly average, D_p < 10 μm, fitted f(RH) data from the SGP CART site. The x axis shows day of the year, 1999. (bottom) Statistical analysis showing hourly average, D_p < 10 μm, fitted f(RH) data over the 4-year period sorted by hour of the day. The ends of the box, the ends of the whiskers, and the line across each box represent the 25th and 75th percentiles, the 5th and 95th percentiles, and the median, respectively. The distribution at the far right of each plot represents all hourly data, and the median line for that distribution is drawn across the entire plot. The vertical line at 1800 UTC is for local noon (1200 LT).

Unfortunately, because of the lack of aerosol chemical data for 1999 we cannot state for certain that we sampled either dust or smoke. Rather, we take the approach that aerosols with the highest large-particle fraction would be indicative of a larger-than-normal contribution of local soil dust and aerosols with the lowest ω_0 (or the darkest aerosols) would indicate a smoke component from the local field fires. These are consistent with typical characteristics of these types of aerosols [e.g., *Hobbs et al.*, 1997]. Hourly average observations of f(RH), when R_{sp} < 0.6 (indicating a significant large particle influence) and ω_0 < 0.8 (darker aerosols), were extracted from the 1999 data set and plotted as frequency distributions in Figure 7. The medians of these subset populations both fell below 1.6, appreciably lower than the 1.83 value for the entire yearly data set. It appears that aerosols containing higher fractions of larger and/or darker particles show lower hygroscopic growth factors, which is consistent with the previous observations of the humidity dependence of particle growth for dust and smoke aerosols.

As shown in Figure 6, the major period of extended low-f(RH) measurements at SGP in 1999 occurred during Julian days 296–299 (October 23–26, 1999), when the f(RH) varied between ~1.0 and 1.5. This period was characterized by above average CN (mean of ~6400 cm^{-3}) and σ_{ap} (~3.2 Mm^{-1}) and below average σ_{sp} (~19 Mm^{-1}), ω_0 (~0.86), and $\mathring{a}$ (~1.3). These low-f(RH), AOP data suggest that combustion aerosols, possibly from local field burning episodes, were a significant component of the sampled aerosols at this time. Analysis of the site visual observations and meteorological records for this time period indicates a few field fires in close proximity to the Central Facility. There were, however, no meteorological observations for 34 of the 72 hours, and nearly half of the observations were taken in the dark, when smoke would be difficult to observe visually. Our conclusion is that the meteorological observation database is of limited usefulness when trying to reconstruct the prevalence of smoke or fires in the area surrounding the SGP CF.

Other dips in the 1999 record often correspond to either local agricultural burning activities or windblown dust episodes on the basis of the meteorological observations. The keywords "smoke," "fires," and "burning" were used to search the database, and other searches were conducted by wind speed to identify likely dust episodes based on high wind speeds. Again, the database is not complete so that a rigorous comparison of hourly meteorological observations with f(RH) would not be productive, but searching on

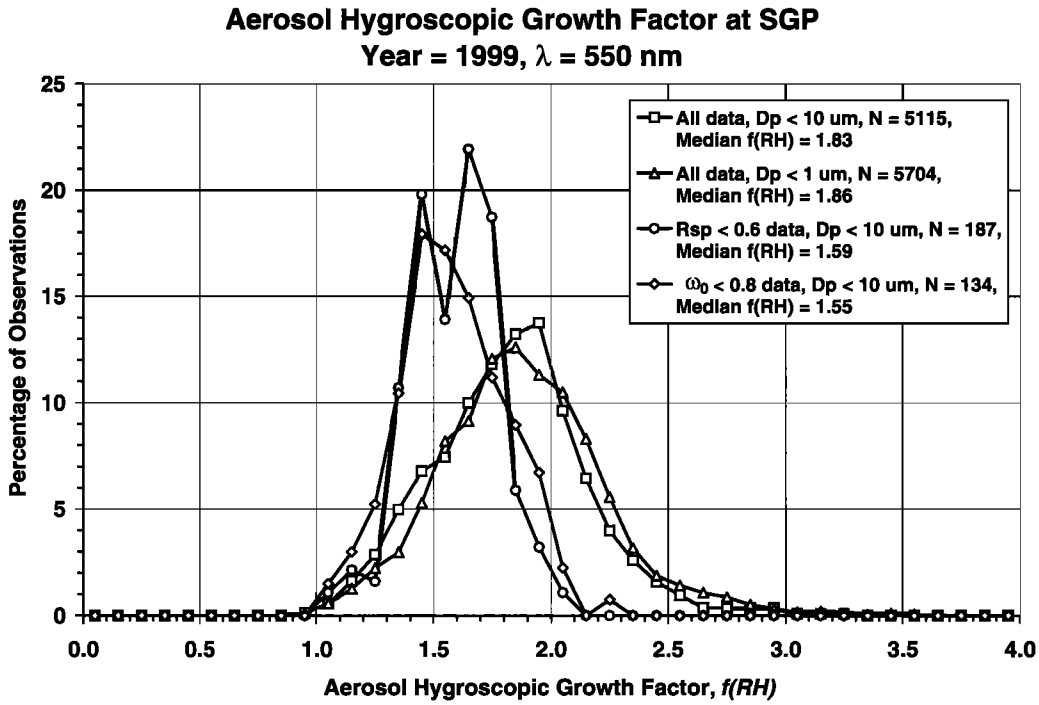

Figure 7. Frequency distributions of hourly average fitted f(RH) data. D_p < 10 μm and D_p < 1 μm aerosol data show similar median f(RH) values (1.83 and 1.86, respectively). Data from periods that were probably influenced by dust (R_{sp} < 0.6) and smoke (ω_0 < 0.8) aerosols show considerably lower median f(RH) values, at 1.59 and 1.55, respectively.

a case-by-case can provide interesting results. Some of the lowest values of f(RH) at <1.3 were observed during windy periods at the SGP CF, which supports the possibility that fresh windblown dust aerosols are hydrophobic and do not show much particle growth until aged and processed by the atmosphere.

4. Summary and Conclusions

Aerosol optical and microphysical property data from the first 4 years of operation of the Aerosol Observing System at the Southern Great Plains CART site Central Facility have been presented. Analysis of these aerosol data, SGP CF meteorological records, and personal observations indicates there is a complex mix of aerosol types frequently present at the site, including dust and smoke aerosols. We have attempted to identify periods when the ambient aerosols were significantly impacted by dust and smoke by their optical properties, although an accurate apportionment can only be achieved through aerosol chemical analysis, which started recently at the site.

Median values of some important aerosol optical properties over the 4-year study are σ_{sp}, 33 Mm^{-1}; σ_{ap} 1.5 Mm^{-1}; ω_0, 0.95; b, 0.13; å, 2.0; and R_{sp}, 0.85. The median f(RH) value for 1999 is 1.83. Four-year time series of hourly average aerosol data show no striking long-term trends, with the exceptions of σ_{ap}, ω_0, and R_{sp} (the trend in the optical particle counter data is considered questionable). Aerosol light absorption appears to have increased and become more variable at least through early 2000, possibly due to increased agricultural burning in the vicinity of the SGP Central Facility. A linear fit of the 4-year data series shows that ω_0 has decreased by $\sim$1–2% yr^{-1}. The ω_0 measurements from early 2000 and our more recent unpublished data indicate higher values for ω_0 than in late 1999, so the recent downward trend in ω_0 may be reversing itself. Clearly, more measurements and a longer time series are needed to document any long-term trend.

Major light scattering and absorption episodes were identified in the aerosol record and were attributed to long-range transport of smoke from the Central American fires of 1998 and the major local field burning episodes of late 1999 and early 2000. The optical properties of these smokes measured at the site were quite different. The Central American smoke was not nearly as dark as local smoke and showed a large scattering peak. Local smoke aerosols typically showed an increase of 5–10 times or more in σ_{ap} and a very low ω_0 (often <0.85), with a more modest increase in σ_{sp}.

A strong daily cycle in the hourly average CN data was observed, with peak particle concentrations in the afternoon and early evening hours. Possible explanations for the high concentrations include buildup and advection of pollutant aerosols from local sources or photochemical particle production. Chemical analyses of aerosol filter samples should help to identify the particles responsible for the high aerosol episodes. The concentration of particles between 0.1 and 10 μm shows a weak, broad peak in the midmorning hours. This peak is similar to the one observed for σ_{sp}, which is expected because the instruments are sensitive to particles in the same size range. The daily cycles of ω_0 and σ_{ap} were also quite similar, with peaks of one distribution matching valleys in the other. This suggests that the variability in ω_0 is driven more by the variability in σ_{ap} than by that in σ_{sp}.

While the data show that aerosol parameters did not vary much by day of the week, the monthly plots showed considerable variability. Slight dips in the median $å$, b, R_{sp}, and a strong peak in 0.1–10 μm particles in the summer all support the possibility of an increase in the fraction of larger particles present at that time. An autumn decrease in ω_0 was observed for the 3 years in the record with autumn ω_0 data, which may be related to regional-scale agricultural or transportation activities or to large-scale changes in atmospheric flow patterns.

We have presented a 1-year record of the aerosol hygroscopic growth factor at the SGP CF. This record is one of the few in the literature of such duration. By the end of 2000, this continuous record will exceed 2 years in length and will then be the longest such record of aerosol hygroscopic growth that we know of. The aerosols over the SGP site typically were very hygroscopic, with a 4-year median f(RH) value of 1.83. The influence of smoke and dust aerosols, which were identified by the change in aerosol optical properties, was to make the aerosols less hygroscopic and lowered the ambient f(RH) values at these times to median values of 1.55 and 1.59, respectively.

These surface aerosol measurements can be used to constrain aerosol optical property values used in column radiative forcing calculations. An upcoming task will be for us to compare the surface measurements with long-term measurements of in situ AOPs collected on board a light aircraft flying over the CART site. This comparison will permit us to determine the extent to which, and under what conditions, surface aerosol properties represent the overlying atmospheric column. Upon observation of the thickness and frequency of the smoke plumes drifting over the Central Facility, we must raise the question of what their impact might be on some column radiation measurements. Because of the limited mixing height of the smoke plumes (and dust clouds) they may not significantly influence column measurements, but then they could be responsible for a major source of disagreement between in situ surface and higher-altitude measurements made either remotely from the surface or by airborne research platforms. More research is necessary to ascertain the effects of fires and windblown dust on SGP CART site measurements.

Acknowledgments. We wish to thank the Department of Energy's Atmospheric Radiation Measurements Program for funding this project. In addition, we thank Jim Teske and the staff of the Southern Great Plains CART Central Facility for the excellent technical support. Thanks are also due Robert Leifer for the initial AOS design and construction, Richard Eagan for the computer data acquisition and system control, and Jim Wendell for the design and fabrication of several AOS control and interface units.

References

Anderson, T. L., and J. A. Ogren, Determining aerosol radiative properties using the TSI 3563 integrating nephelometer, *Aerosol Sci. Technol*, *29*, 57–69, 1998.

Anderson, T. L., et al., Performance characteristics of a high-sensitivity, three-wavelength, total scatter/backscatter nephelometer, *J. Atmos. Oceanic Technol.*, *13*, 967–986, 1996.

Andrews, E., P. J. Sheridan and J. A. Ogren, In-situ aerosol profiles over the Southern Great Plains CART site, paper presented at the ARM Science Team Annual Meeting, Dep. of Energy, Atmos. Radiat. Meas. Program, Atlanta, Ga., Mar. 19–23, 2001.

Bond, T. C., T. L. Anderson, and D. Campbell, Calibration and intercomparison of filter-based measurements of visible light absorption by aerosols, *Aerosol Sci. Technol.*, *30*, 582–600, 1999.

Carrico, C. M., M. J. Rood, and J. A. Ogren, Aerosol light scattering properties at Cape Grim, Tasmania, during the first Aerosol Characterization Experiment (ACE 1), *J. Geophys. Res.*, *103*, 16,565–16,574, 1998.

Charlson, R. J., S. E. Schwartz, J. M. Hales, R. D. Cess, J. A. Coakley, Jr., J. E. Hansen, and D. J. Hofmann, Climate forcing by anthropogenic aerosol, *Science*, *255*, 423–430, 1992.

Covert, D. S., R. J. Charlson, and N. C. Ahlquist, A study of the relationship of chemical composition and humidity to light scattering by aerosols, *J. Appl Meteorol.*, *11*, 968–976, 1972.

Friedlander, S. K., *Smoke, Dust and Haze· Fundamentals of Aerosol Behavior*, pp. 114–118, John Wiley, New York, 1977.

Gassó, S., et al., Influence of humidity on the aerosol scattering coefficient and its effect on the upwelling radiance during ACE-2, *Tellus, Ser. B*, *52*, 546–567, 2000.

Haywood, J. M., and K. P. Shine, The effect of anthropogenic sulfate and soot aerosol on the clear sky planetary radiation budget, *Geophys. Res. Lett.*, *22*, 603–606, 1995.

Hobbs, P. V., J. S. Reid, R. A. Kotchenruther, R. J. Ferek, and R. Weiss, Direct radiative forcing from biomass burning, *Science*, *275*, 1776–1778, 1997.

Hofmann, D., and J. Peterson (Eds.), *Summary Report 24, 1996–1997*, Clim. Monit. and Diagnostics Lab., Boulder, Colo., Dec. 1998.

Intergovernmental Panel on Climate Change (IPCC), *Climate Change 1995: The Science of Climate Change*, edited by J. T. Houghton et al., pp. 18–25, Cambridge Univ. Press, New York, 1996.

Kiehl, J. T., and B. P. Briegleb, The relative roles of sulfate aerosols and greenhouse gases in climate forcing, *Science, 260*, 311–314, 1993.

Kim, Y. J., Response of the active scattering aerosol spectrometer probe (ASASP-100X) to particles of different chemical composition, *Aerosol Sci. Technol., 22*, 33–42, 1995.

Kotchenruther, R. A., and P. V. Hobbs, Humidification factors of aerosols from biomass burning in Brazil, *J. Geophys. Res., 103*, 32,081–32,089, 1998.

Li-Jones, X., H. B. Maring, and J. M. Prospero, Effect of relative humidity on light scattering by mineral dust aerosol as measured in the marine boundary layer over the tropical Atlantic Ocean, *J. Geophys. Res., 103*, 31, 113–31, 121, 1998.

Penner, J. E., R. J. Charlson, J. M. Hales, N. S. Laulainen, R. Leifer, T. Novakov, J. Ogren, L. F. Radke, S. E. Schwartz, and L. Travis, Quantifying and minimizing uncertainty of climate forcing by anthropogenic aerosols, *Bull. Am. Meteorol. Soc., 75*, 375–400, 1994.

Peppler, R. A., et al., ARM Southern Great Plains site observations of the smoke pall associated with the 1998 Central American fires, *Bull. Am. Meteorol. Soc., 81*, 2563–2591, 2000.

Rood, M. J., D. S. Covert, and T. V. Larson, Hygroscopic properties of atmospheric aerosol in Riverside, California, *Tellus, Ser. B, 39*, 383–397, 1987.

Stokes, G. M., and S. E. Schwartz, The Atmospheric Radiation Measurement (ARM) Program: Programmatic background and design of the cloud and radiation testbed, *Bull. Am. Meteorol. Soc., 75*, 1201–1221, 1994.

Wiscombe, W. J., and G. W. Grams, The backscattered fraction in two-stream approximations, *J. Atmos. Sci., 33*, 2440–2451, 1976.

D. J. Delene, J. A. Ogren, and P. J. Sheridan, Climate Monitoring and Diagnostics Laboratory, NOAA, 325 Broadway, Boulder, CO 80303, USA. (jogren@cmdl.noaa.gov; patrick.sheridan@noaa.gov)

(Received October 26, 2000; revised March 20, 2001;
accepted April 18, 2001.)